The 2010 IEEE/RSJ International Conference on
Intelligent Robots and Systems
October 18-22, 2010, Taipei, Taiwan

3-D Biped Walking over Rough Terrain based on the Assumption of Point-contact

Tadayoshi Aoyama, Kosuke Sekiyama, Yasuhisa Hasegawa, and Toshio Fukuda

Abstract— **This paper describes a 3-D biped walking over rough terrain. The robot is modeled as the special 3-D inverted pendulum that can change the length. The dynamics of the 3-D inverted pendulum is modeled as 2-D autonomous system by applying the Passive Dynamic Autonomous Control (PDAC) that is based on the assumption of point-contact of the robot foot and the virtual holonomic constraint as to robot joints. We analyze the stability of the 2-D autonomous system by use of Poincaré map, and derive the stable range over rough terrain. By applying the virtual compliance control to an actual robot "Gorilla Robot Ⅲ", the angle of the pendulum is modified. Finally, the 3-D biped walking over rough terrain is realized by use of the Gorilla Robot Ⅲ.**

I. INTRODUCTION

A number of humanoid robots have been explored as a recent progress of robot technologies [1], [2]. These robots can walk on two legs stably by means of the control based on Zero-Moment Point (ZMP) [3]. Some humanoid robots realized three-dimensional biped walking by use of the ZMP-based control scheme even if a terrain is not flat [4], [5]. However, the ZMP-based does not use an inherent dynamics of the robot to realize a natural and efficient walking.

In contrast, so as to realize a natural and efficient walking, some researchers proposed methods to utilize the robot dynamics directly, assuming a point-contact between the robot foot and the ground. Some of these point-contact methods realized smooth dynamic walking with two-dimensional experimental robots [6], [7]. Also, it is reported that the planar experimental robot realized dynamic walking over rough terrain [8]. In this work, the provably-stable controller was developed over uneven terrain based on the general method of exponentially stabilizing arbitrary motions of underactuated systems.

Some interesting three-dimensional bipedal walking control law based on point-contact method have been proposed [9], [10]; however, few works have conducted the experiments with an actual robot. Miura and Shimoyama presented a stilt-like biped and the control method to stabilize the gaits by changing the robot posture at foot-contact and realized three-dimensional walking with the experimental robot [11]. Its step length has to be quite small since the robot has no trunk and the controller is based on linearization. Doi *et al.* proposed Passive Dynamic Autonomous Control (PDAC) [12] which is one of the point-contact methods and realized three-dimensional dynamic walking with the experimental robot based on the assumption that the sagittal and lateral motion can be separated [13]. This control method has problems in dividing three-dimensional dynamics when the dynamics of each plane are closely coupled. In order to solve this problem, we extended the PDAC approach further to three-dimensional dynamics without dividing and proposed the stabilizing method and walking direction control of a three-dimensional biped walking [14]. In this work, the efficiency of the proposed control algorithm was verified by using an actual robot "Gorilla Robot Ⅲ [15]" on a flat terrain. Though the realization of bipedal walking in the work [14] indicates a certain amount of walking ability, the analysis of walking adaptability has not been conducted.

The motivation of this study is to analyze environmental adaptability of point-contact method and realize experimentally three-dimensional biped walking on a non-flat ground. The robot is modeled as the special three-dimensional inverted pendulum that can change the length. The dynamics of the three-dimensional inverted pendulum is modeled as two-dimensional autonomous system by applying PDAC concept. We analyze the stability of the two-dimensional autonomous system by use of Poincaré map, and derive the stable range over rough terrain. By applying the virtual compliance control to an actual robot Gorilla Robot Ⅲ, the angle of the pendulum is modified. Finally, the three-dimensional biped walking over rough terrain is realized by use of the Gorilla Robot Ⅲ.

II. WALKING MODEL

A. 3-D inverted pendulum model

In this paper, a robot is modeled as a three-dimensional inverted pendulum as shown in Fig. 1(a) that is same as our previous work [14]. We apply an assumption of the point-contact to this pendulum in accordance with the PDAC [12], hence it is possible to choose the axes of pendulum angle around the contact point to express its motion. We utilize the polar coordinate system. The state variables and parameters are shown in Fig. 2(b). Angles ϕ and θ are the variables of the pendulum inclination around the contact point. Joint angles q_1, q_2, and q_3 decide the upper body posture. l is the variable of the pendulum length. L is the virtual value for convenience of description and equals zero. By use of the six variables ϕ, θ, q_1 to q_3, and l, it is possible to express any states of the robot.

This work was supported by JSPS (Grant-in-Aid for JSPS Fellows).

T. Aoyama and K. Sekiyama and T. Fukuda are with the Department of Micro-Nano Systems Engineering, Nagoya University, Furo-cho-1, Chikusa-ku, Nagoya, 464-8603, JAPAN aoyama@robo.mein.nagoya-u.ac.jp; sekiyama@mein.nagoya-u.ac.jp; fukuda@mein.nagoya-u.ac.jp

Y. Hasegawa is with the Department Intelligent Interaction Technologies, University of Tsukuba, 1-1-1 Tenodai, Tsukuba, 305-8573, JAPAN hase@esys.tsukuba.ac.jp

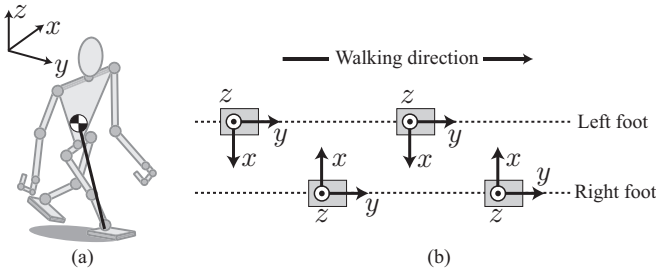

Fig. 1. (a) 3-D inverted pendulum model. (b) Definition of coordinate system Note that this figure shows just a coordinate system definition and doesn't mean that foot placement is in alignment.

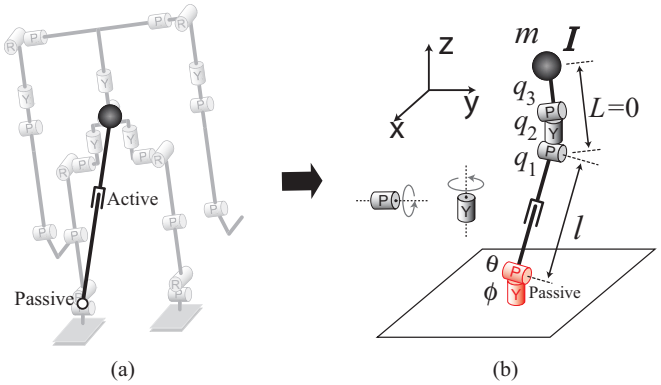

Fig. 2. (a) Passive joints (point-contact) and active pendulum length actuation. (b) Parameters and variables of the 3-D inverted pendulum model.

The left-handed system is used in the left-leg supporting phase and vice versa as shown in Fig. 1(b), so that it is possible to describe the robot dynamics in both supporting phases as a single dynamics.

B. Converged dynamics with PDAC

In this paper, the trunk inclination is kept in the gravitational direction and the upper body does not rotate around yaw-axis, that is,

$$q_1 = -\theta, \tag{1}$$
$$q_2 = -\phi, \tag{2}$$
$$q_3 = 0. \tag{3}$$

In addition, we assume that the robot is symmetrical. By applying PDAC, dynamic equations of 3-D inverted pendulum are expressed as follows:

$$\frac{d}{dt}\left(ml^2 \sin^2\theta\dot{\phi}\right) = 0, \tag{4}$$
$$\frac{d}{dt}\left(ml^2\dot{\theta}\right) = ml^2\dot{\phi}^2 \sin\theta\cos\theta + mgl\sin\theta. \tag{5}$$

The detailed calculation process of (4) and (5) is given in [16]. By multiplying both sides of (4) by $ml^2\sin^2\theta\dot{\phi}$, and integrating with respect to time, the following converged dynamics is obtained,

$$\dot{\phi} = \frac{\sqrt{2C_1}}{ml^2\sin^2\theta} \tag{6}$$
$$:= Z_1(\theta), \tag{7}$$

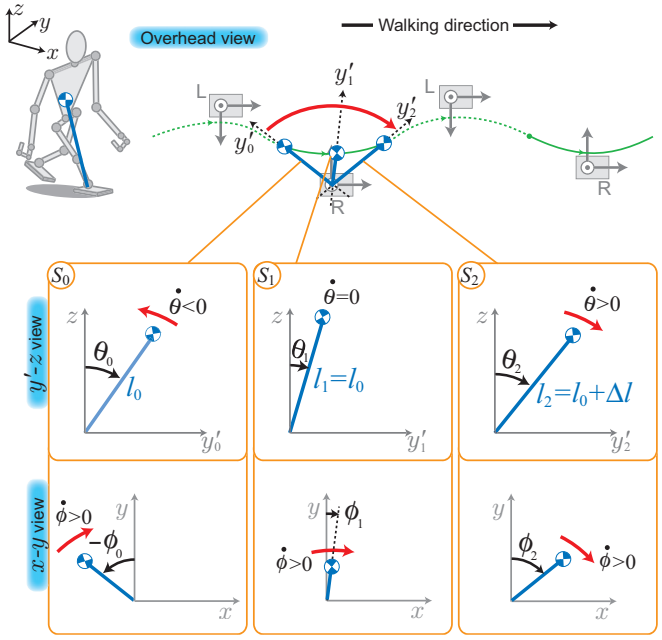

Fig. 3. Parameters and variables of dynamic walking based on 3D inverted pendulum model.

where C_1 is the integral constant which is determined by initial state immediately after foot-contact. Substituting (6) into (5) results in

$$\dot{\theta} = \frac{1}{ml^2}\sqrt{2\int\left(\frac{2C_1\cos\theta}{\sin^3\theta} + m^2gl^3\sin\theta\right)d\theta} \tag{8}$$
$$:= \frac{1}{M(\theta)}\sqrt{2\big(D(\theta)+C_2\big)} \tag{9}$$
$$:= Z_2(\theta). \tag{10}$$

Next, in accordance with PDAC, the pendulum length is described as the function of θ,

$$l := \lambda(\theta). \tag{11}$$

In this paper, λ is defined as the following function of θ,

$$\lambda(\theta) =: \sqrt[3]{p_1\theta^3 + p_2\theta^2 + p_3\theta + p_4} \tag{12}$$
$$=: \sqrt[3]{f(\theta)}, \tag{13}$$

where p_1-p_4 are the coefficients decided by the extended length of the pendulum and the condition of continuity.

By substituting this equation into (8), the converged dynamics is derived,

$$M(\theta) = mf(\theta)^{2/3} \tag{14}$$
$$D(\theta) = -\frac{C_1}{\sin^2\theta} - m^2g\Big(\big(f(\theta)-f''(\theta)\big)\cos\theta - \big(f'(\theta)-f'''(\theta)\big)\sin\theta\Big). \tag{15}$$

Fig. 3 shows the parameters and variables of the pendulum motion. S_0 and S_2 denote moments just before and after a foot-contact, and S_1 is a moment at $\dot{\theta} = 0$. θ_i, ϕ_i, and l_i denote the roll angle, yaw angle, and pendulum length at S_i $(i = 0, 1, 2)$ respectively. During a cycle of walking motion, ϕ is monotonically increasing. Meanwhile, θ decreases at first, and then increases, after posing for a moment at θ_1.

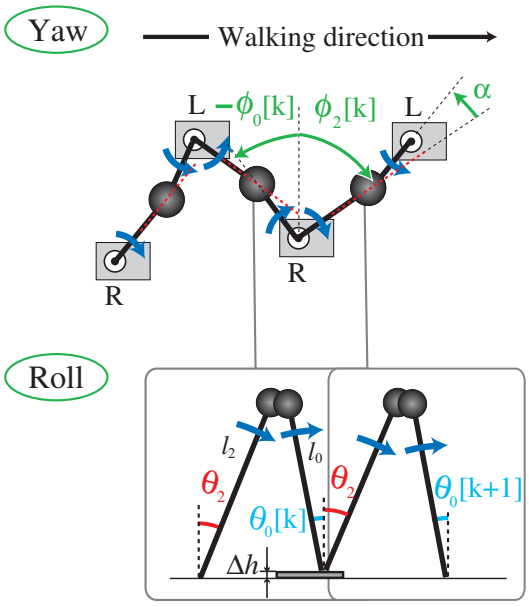

Fig. 4. Geometrical constraints at foot-contact.

C. Foot-contact model

In this paper, it is assumed that there is an uneven step with the Δh height at kth step. Fig. 4 shows the geometric condition at a foot-contact. Yaw angle of a swing-leg is shifted by α from the symmetrical position with a stance-leg at a foot-contact, i.e. it is $\phi_0[k+1] = -\phi_2[k] + \alpha$, where $\phi_0[k+1]$ and $\phi_2[k]$ denote ϕ_0 and ϕ_2 at $k+1$th and kth step respectively. At a foot-contact, l_0, l_2, and θ_2 are set to constant value, that is, COG height of just before a foot-contact, $h = l_2 \cos\theta_2$ is constant. Also, it is assumed that θ_0 is valuable decided by the uneven height Δh. Then, we can get the following equation:

$$\begin{cases} h = l_0 \cos\left(\theta_0[k]\right) + \Delta h & (16) \\ h = l_0 \cos\left(\theta_0[k+1]\right) - \Delta h. & (17) \end{cases}$$

In this paper, perfectly inelastic collision is assumed between the ground and a foot occurs for a moment, same as our previous work [14]. Since angular momentum around a new contact point is conserved, the yaw and roll angular velocity of the pendulum just after $k+1$th foot-contact, $\dot{\phi}_0[k+1]$ and $\dot{\theta}_0[k+1]$ are derived as follows from (7), (10) and the assumption of the perfectly inelastic collision:

$$\dot{\theta}_0[k+1] = \frac{l_2}{l_0}\Big(\dot{\theta}_2[k]\big(\sin\theta_2 \sin(\theta_0[k+1]) - \cos(\theta_0[k+1]) \cos\theta_2 \cos\alpha\big) + \dot{\phi}_2[k] \cos(\theta_0[k+1]) \sin\theta_2 \sin\alpha\Big), \quad (18)$$

$$\dot{\phi}_0[k+1] = \frac{l_2}{l_0 \sin(\theta_0[k+1])}\Big(\dot{\theta}_2[k] \cos\theta_2 \sin\alpha + \dot{\phi}_2[k] \sin\theta_2 \cos\alpha\Big), \quad (19)$$

where $\phi_0[k+1]$ and $\theta_0[k+1]$ are the yaw and roll angle just after $k+1$th foot-contact, $\dot{\phi}_2[k]$ and $\dot{\theta}_2[k]$ are the yaw and roll angler velocity just before $k+1$th foot-contact, ϕ_2 and θ_2 are the yaw and roll angle just before a foot-contact (see Fig. 3 and Fig. 4).

III. STABILITY ANALISIS

A. Poincaré map of the walking cycle

In this paper, the walking cycle is expressed as a nonlinear discrete system with a foot-contact; then the stability analysis around the fixed point is conducted by use of Poincaré map. $\dot{\phi}$ and $\dot{\theta}$ just after kth foot-contact that compose the autonomous system (7) and (10) are selected as discrete state:

$$\boldsymbol{v}_k = \begin{bmatrix} \dot{\phi}_0[k] \\ \dot{\theta}_0[k] \end{bmatrix}. \quad (20)$$

From (6) and (9) the angular velocities of $k+1$th step just before a foot-contact $\dot{\phi}_2[k]$, $\dot{\theta}_2[k]$ are derived as follows:

$$\dot{\phi}_2[k] = \frac{\sqrt{2C_1}}{ml_2^2 \sin\theta_2}, \quad (21)$$

$$\dot{\theta}_2[k] = \frac{1}{M(\theta_2)}\sqrt{2\big(D(\theta_2) + C_2\big)}, \quad (22)$$

where C_1 and C_2 are conservative quantities that conserve during a single support phase. C_1 and C_2 are derived from (6), (8) using the discrete state of kth step as follows:

$$C_1 = \frac{1}{2}\left(\dot{\phi}_0[k] m l_0^2 \sin(\theta_0[k])\right)^2 := \xi_1(\dot{\phi}_0[k]), \quad (23)$$

$$C_2 = 2(ml_0^2\dot{\theta}_0[k])^2 + \frac{C_1}{\sin^2(\theta_0[k])} + m^2 g l_0 \cos(\theta_0[k]) := \xi_2(\dot{\phi}_0[k], \dot{\theta}_0[k]). \quad (24)$$

By substituting (23) and (24) into (21) and (22), $\dot{\phi}_2[k]$ and $\dot{\theta}_2[k]$ are expressed as follows:

$$\dot{\phi}_2[k] = \frac{\sqrt{2\xi_1}}{ml_2^2 \sin^2\theta_2}, \quad (25)$$

$$\dot{\theta}_2[k] = \frac{1}{ml_2^2}\sqrt{2\left(\frac{-\xi_1}{\sin^2\theta_2} - m^2 g l_2 \cos\theta_2 + \xi_2\right)}. \quad (26)$$

From (16) and (17), $\theta_0[k]$ and $\theta_0[k+1]$ are expressed by use of Δh:

$$\begin{cases} \theta_0[k] = \arccos\left(\dfrac{h - \Delta h}{l_0}\right) & (27) \\ \theta_0[k+1] = \arccos\left(\dfrac{h + \Delta h}{l_0}\right). & (28) \end{cases}$$

From (18), (19), (25), (26), (27), and (28), the discrete state of $k+1$th step is described as the function of the discrete state of kth step and Δh,

$$\dot{\phi}_0[k+1] = \frac{l_2}{\sqrt{l_0^2 - (h+\Delta h)^2}} \left[\frac{h \sin\alpha}{ml_0^2 l_2}\sqrt{W_1\left(\dot{\phi}_0[k], \dot{\theta}_0[k], \Delta h\right)} + W_2\left(\dot{\phi}_0[k], \Delta h\right)\cos\alpha\right] \quad (29)$$

$$\dot{\theta}_0[k+1] = \frac{l_2}{l_0}\left[\frac{1}{ml_2^2}\left(\sqrt{\left\{1-\frac{(h+\Delta h)^2}{l_0^2}\right\}\left\{1-\left(\frac{h}{l_0}\right)^2\right\}} - \frac{h(h+\Delta h)}{l_0}\cos\alpha\right)\sqrt{W_1\left(\dot{\phi}_0[k],\dot{\theta}_0[k],\Delta h\right)} + W_2\left(\dot{\phi}_0[k],\Delta h\right)\frac{h+\Delta h}{l_0}\sin\alpha\right], \quad (30)$$

where

$$W_1\left(\dot{\phi}_0[k],\dot{\theta}_0[k],\Delta h\right) = 2\left\{C_1[k]\left(\frac{l_0^2}{l_0^2-(h-\Delta h)^2}-\frac{l_2^2}{l_2^2-h^2}\right)\right\} + m^2 g\Delta h + 2\left(ml_0^2\dot{\theta}_0[k]\right)^2, \quad (31)$$

$$W_2\left(\dot{\phi}_0[k],\Delta h\right) = \dot{\phi}_0[k]\frac{(h+\Delta h)^2}{l_2}\sqrt{\frac{1}{l_2^2-h^2}}\ . \quad (32)$$

By defining the vector function $\boldsymbol{P}$ from (29) and (30), Poincaré map is described as follows:

$$\boldsymbol{v}_{k+1} = \boldsymbol{P}\left(\boldsymbol{v}_k\right). \quad (33)$$

Especially, if the state of the walking cycle converge to fixed point $\boldsymbol{v}^*$, the following equation is derived,

$$\boldsymbol{v}^* = \boldsymbol{P}\left(\boldsymbol{v}^*\right). \quad (34)$$

Considering Taylor developing around the fixed point,

$$\boldsymbol{v}^* + \delta\boldsymbol{v}_{k+1} = \boldsymbol{P}\left(\boldsymbol{v}^* + \delta\boldsymbol{v}_k\right) \approx \boldsymbol{P}\left(\boldsymbol{v}^*\right) + \boldsymbol{J}\left(\boldsymbol{v}^*\right)\delta\boldsymbol{v}_k, \quad (35)$$

where $\boldsymbol{J}\left(\boldsymbol{v}^*\right)$ is Jacobian matrix at the fixed point, $\delta\boldsymbol{v}$ is the small displacement vector. Thus, if all of the eigenvalues of the Jacobian matrix $\boldsymbol{J}\left(\boldsymbol{v}^*\right)$ are inside the unit circle on the complex plane, the walking cycle is asymptotically stable.

B. Stability analysis

First of all, we analyze the stability of the walking model explained in the section II on a flat terrain, that is, $\Delta h = 0$. By numerical simulation, the fixed point $\boldsymbol{v}^*$ of this walking model when the parameters are set as $h = 0.541$, $l_0 = 0.56$, $l_2 = 0.561$, $\alpha = 0.035$ is calculated as follows:

$$\boldsymbol{v}^* = \begin{bmatrix} 0.9504 \\ -1.140 \end{bmatrix}. \quad (36)$$

By numerical calculation, Jacobian matrix $\boldsymbol{J}\left(\boldsymbol{v}^*\right)$ is also calculated as follows:

$$\boldsymbol{J}\left(\boldsymbol{v}^*\right) = \begin{bmatrix} 0.8230 & -0.1298 \\ -0.0044 & 0.8155 \end{bmatrix}. \quad (37)$$

The eigenvalues λ_1, λ_2 of the Jacobian matrix $\boldsymbol{J}\left(\boldsymbol{v}^*\right)$ are obtained numerically as $\lambda_1 = 0.8435, \lambda_2 = 0.7949$. Since all of the eigenvalues are less than 1, the designed walking cycle is asymptotically stable on a flat terrain. Fig. 6 shows the simulation result of this condition. From this figure, it is confirmed that $\dot{\theta}$ and $\dot{\phi}$ converge to a certain fixed point.

Next, same stability analysis is conducted on rough terrains. In this analysis, the eigenvalues are calculated when the Δh is changed every 1 [mm]. In Fig. 5, some of the eigenvalues are plotted on the complex plane. From the stability analysis, the designed walking model on the condition of these parameters is asymptotically stable when the Δh is -50 [mm] to 8[mm]; in the range, the state of the walking cycle converge to fixed point of the flat terrain $\boldsymbol{v}^*$. More stability analysis confirmed that the asymptotically stable range depends on the setting parameters. The result introduced in this section is one example that can be applied to the Gorilla Robot Ⅲ [15] explained in the section IV-B. Optimization of the parameters to maximize the stable range is one of the future works.

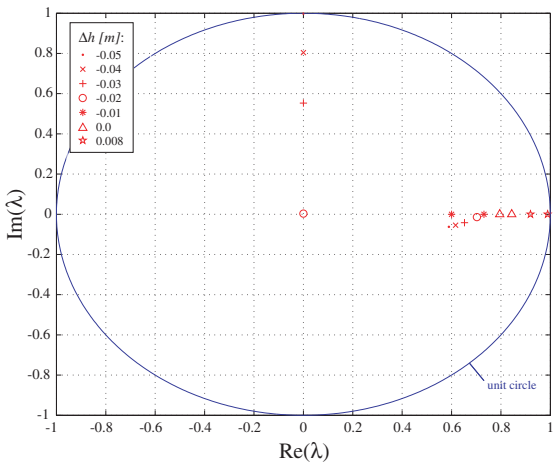

Fig. 5. Eigenvalues of the Jacobian.

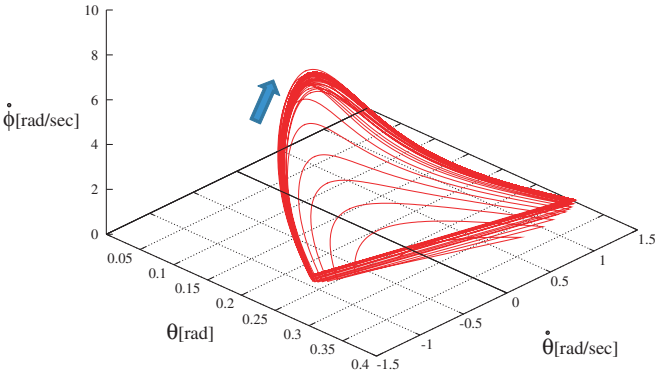

Fig. 6. Phase Portrait.

IV. EXPERIMENT

A. Control architecture using the virtual compliance control

In the experiment, the position and posture of the 3-D inverted pendulum modeled in the section II-A are derived every control step from converged dynamics (7), (10), and the constraint (1)-(3). By use of inverse kinematics, all the joint angles of the experimental robot are calculated and controlled every control step. In this paper, it is assumed point-contact of the robot foot; however most of humanoid type robots include the Gorilla Robot Ⅲ [15] (It is introduced in the next subsection.) have feet. In this research, the ankle joints

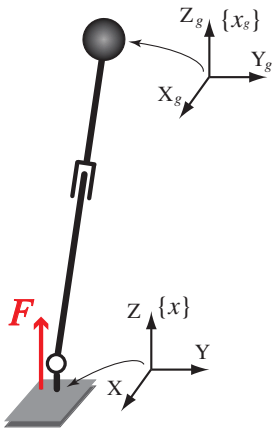

Fig. 7. Coordinate System.

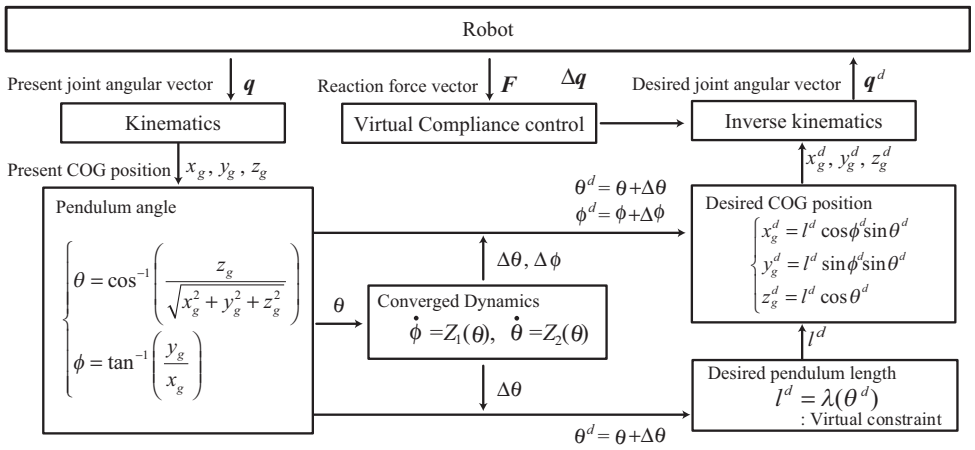

Fig. 8. Control Architecture.

are decided by dynamics (7), (10), and the constraint (1)-(3) base on the assumption that the terrain is flat ($\Delta h = 0$). Therefore, by applying the virtual compliance control to ankle actuators, the pendulum angles of the foot-contact are changed in accordance with the ground irregularity Δh. In this research, the virtual compliance control is applied same as the work [17]. The condition that foot realizes the virtual compliance is expressed as follows:

$$\boldsymbol{F} = \boldsymbol{K}\Delta\boldsymbol{x} + \boldsymbol{C}\dot{\boldsymbol{x}}, \tag{38}$$

where $\boldsymbol{F}$ is the force and moment vectors acting to foot coordinate, $\Delta\boldsymbol{x}$ is the displacement of foot coordinate, and $\dot{\boldsymbol{x}}$ is the velocity of the foot coordinate (see Fig. 7). $K \in \boldsymbol{R}^6$ and $C \in \boldsymbol{R}^6$ are stiffness and damping matrixes. In this work, the purpose of the virtual compliance control is to modify the pendulum angles; thus only roll and pitch angle of the robot foot are considered. From discrete (38), the compliance position of the foot is derived as follows:

$$\Delta\boldsymbol{x}\,(t+\Delta t) = \left[\boldsymbol{K} + \frac{\boldsymbol{C}}{\Delta t}\right]^{-1}\left\{\boldsymbol{F} + \boldsymbol{C}\frac{\Delta\boldsymbol{x}(t)}{\Delta t}\right\}. \tag{39}$$

where Δt is control cycle, $\Delta\boldsymbol{x}\,(t+\Delta t)$ is the present error of foot coordinate from ideal position, $\Delta\boldsymbol{x}(t)$ is the error of foot coordinate from ideal position before one control cycle. The compliance position are add to desired trajectory of the Center of Gravity (COG) derived from converged dynamics (7) and (10), by use of inverse kinematics the desired trajectories of all actuator are modified. This control architecture is shown in Fig. 8.

B. Experimental setup

Fig. 9 depicts the overview of our robot Gorilla Robot Ⅲ(Multi-Locomotion Robot) [15] and its link structure. The robot is approximately 1.0[m] tall, weighs approximately 24.0[kg], and consists of 25 links and 24 motors including two grippers. The real-time operating system VxWorks (Wind River Systems) runs on a Pentium Ⅲ PC for processing sensory data and generating its behaviors. Each joint is driven by AC servo motor through the harmonic drive gear, partially

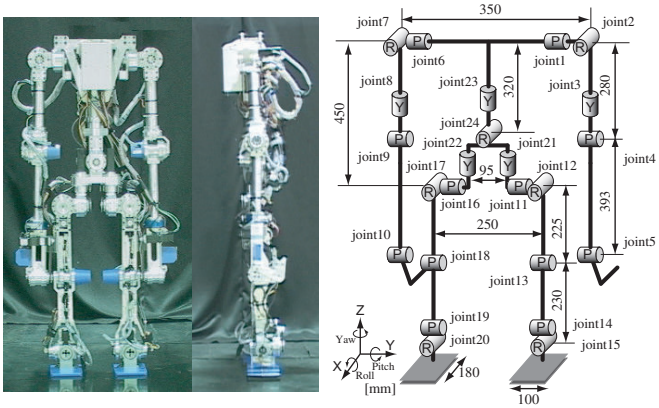

Fig. 9. Gorilla Robot Ⅲ(Multi-Locomotion Robot) [15]. This robot is multi-locomotive; it can perfome biped locomotion, quadruped locomotion and brachiation.

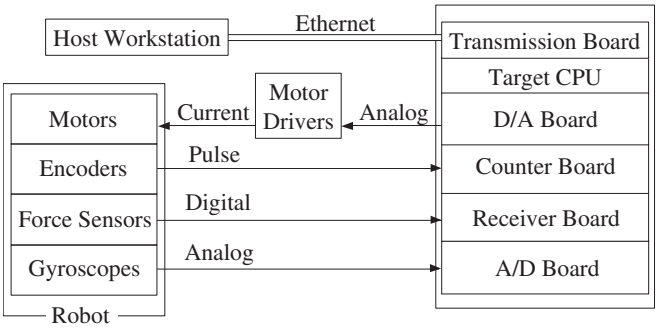

Fig. 10. Control System of Gorilla Robot Ⅲ.

through a timing belt. Maximum output power of the motor is 30[W]. The power supply and the computer are installed outside of the robot for weight saving. The control system of the Gorilla Robot Ⅲ is shown as Fig. 10.

C. Experimental result

We validated the proposed algorithm with the Gorilla Robot Ⅲ. The experiment was carried out on the basis of the condition that the parameters are equal to those used in the stability analysis. The terrain has 3[mm] irregularity

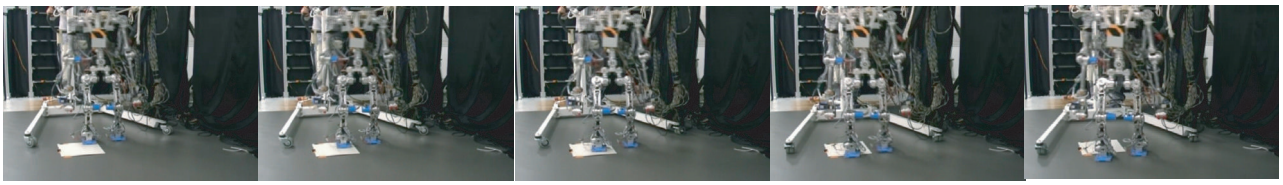

(a) (b) (c) (d) (e)

Fig. 11. Snapshots of the Bipedal Walking Experiment. Each figure shows the snapshots at (a)8th (b)10th (c)12th (d)14th (e)16th step.

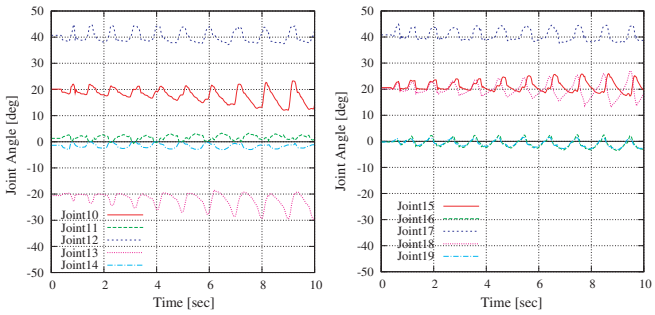

(a)Joint Angles of the Left Leg. (b)Joint Angles of the Right Leg.

Fig. 12. Joint angle of the bipedal walking experiment.

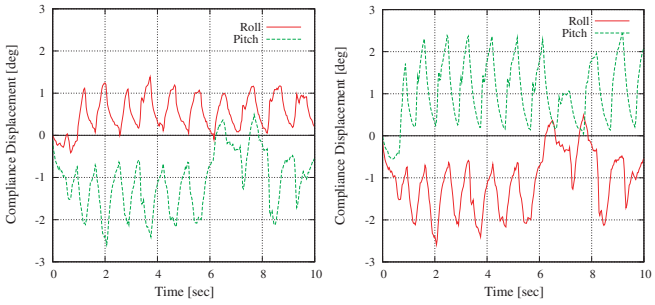

(a)Compliance displacement of the Left Leg. (b)Compliance displacement of the Right Leg.

Fig. 13. Compliance displacement of the bipedal walking experiment.

on the level ground. As a result of the experiment, three-dimensional dynamic walking was realized. Although the ground has 3[mm] irregularity in the experimental environment and the information of the ground shape was not given to the robot, the robot achieved the stable walking without information of the ground. Fig. 11 shows snapshots of the experiment. Also, Fig. 12 and Fig. 13 show the joint angles and compliance displacement of the experiment respectively.

V. CONCLUSIONS

This paper proposed the three-dimensional walking algorithm over the rough terrain. The robot dynamics was modeled as a two-dimensional autonomous system of a three-dimensional inverted pendulum by applying the PDAC concept; then the stability of the two-dimensional autonomous system with foot-contact was analyzed. As the result, the system has an asymptotically stable range due to the parameters. Finally, within the stable range, we experimentally realized a three-dimensional biped dynamic walking on the irregular ground. Optimization of the walking parameters to maximize the stable range is one of the future works.

REFERENCES

[1] K. Hirai, M. Hirose, Y. Haikawa, and T. Takenaka, "The Development of Honda Humanoid Robot," in *Proceedings of the IEEE International Conference on Robotics and Automation*, 1998, pp. 1321–1326.

[2] K. Kaneko, K. Harada, F. Kanehiro, G. Miyamori, and K. Akachi, "Humanoid Robot HRP-3," in *Proceedings of the IEEE/RSJ International Conference on Intelligent Robots and Systems*, 2008, pp. 2471–2478.

[3] M. Vukobratovic and B. Borovac, "ZERO-MOMENT POINT - THIRTY FIVE YEARS OF ITS LIFE," *International Journal of Humanoid Robotics*, vol. 1, no. 1, pp. 157–173, 2004.

[4] H. Hirukawa, S. Hattori, S. Kajita, K. Harada, K. Kaneko, F. Kanehiro, M. Morisawa, and S. Nakaoka, "A Pattern Generator of Humanoid Robots Walking on a Rough Terrain," in *Proceedings of the IEEE International Conference on Robotics and Automation*, 2007, pp. 2181–2187.

[5] T. Takubo, Y. Imada, K. Ohara, Y. Mae, and T. Arai, "Rough Terrain Walking for Bipedal Robot by Using ZMP Criteria Map," in *Proceedings of the IEEE International Conference on Robotics and Automation*, 2009, pp. 788–793.

[6] E. R. Westervelt, G. Buche, and J. Grizzle, "Experimental Validation of a Framework for the Design of Controllers that Induce Stable Walking in Planar Bipeds," *The International Journal of Robotics Research*, vol. 23, no. 6, pp. 559–582, 2004.

[7] S. Kajita, T. Yamaura, and A. Kobayashi, "Dynamic walking control of a biped robot along a potential energy conserving orbit," *IEEE Transactions on Robotics and Automation*, vol. 8, no. 4, pp. 431–438, 1992.

[8] I. R. Manchester, U. Mettin, F. Iida, and R. Tedrake, "Stable DynamicWalking over Rough Terrain Theory and Experiment," in *Proceedings of the International Symposium on Robotics Research*, 2009, pp. 1–16.

[9] G. Song and M. Zefran, "Underactuated Dynamic Three-Dimensional Bipedal Walking," in *Proceedings of the IEEE International Conference on Robotics and Automation*, 2006, pp. 854–859.

[10] C. Chevallereau, J. W. Grizzle, and C.-L. Shih, "Asymptotically Stable Walking of a Five-Link Underactuated 3-D Bipedal Robot," *IEEE Transactions on Robotics*, vol. 25, no. 1, pp. 37–50, 2009.

[11] H. Miura and I. Shimoyama, "Dynamic Walking of a biped," *The International Journal of Robotics Research*, vol. 3, no. 2, pp. 60–74, 1984.

[12] M. Doi, Y. Hasegawa, and T. Fukuda, "Passive Dynamic Autonomous Control of Bipedal Walking," in *Proceedings of the IEEE/RAS International Conference on Humanoid Robots*, 2004, pp. 811– 829.

[13] T. Fukuda, M. Doi, Y. Hasegawa, and H. Kajima, *Fast Motions in Biomechanics And Robotics: Optimization And Feedback Control*. Springer-Verlag, 2006, ch. Multi-Locomotion Control of Biped Locomotion and Brachiation Robot, pp. 121–145.

[14] T. Aoyama, Y. Hasegawa, K. Sekiyama, and T. Fukuda, "Stabilizing and Direction Control of Efficient 3-D Biped Walking Based on PDAC," *IEEE/ASME Transactions on Mechatronics*, vol. 14, no. 6, pp. 712–718, 2009.

[15] T. Fukuda, T. Aoyama, Y. Hasegawa, and K. Sekiyama, *Artificial Life Models in Hardware*. Springer-Verlag, 2009, ch. Multilocomotion Robot: Novel Concept, Mechanism, and Control of Bio-inspired Robot, pp. 65–86.

[16] M. Doi, Y. Hasegawa, and T. Fukuda, "3D Dynamic Walking based on the inverted pendulum model with two degree of underactuation," in *Proceedings of the IEEE/RSJ International Conference on Intelligent Robots and Systems*, 2005, pp. 2788–2793.

[17] K. Hashimoto, A. Hayashi, T. Sawato, Y. Yoshimura, T. Asano, K. Hattori, Y. Sugahara, H. ok Lim, and A. Takanishi, "Terrain-Adaptive Control with Small Landing Impact Force for Biped Vehicle," in *Proceedings of the IEEE/RSJ International Conference on Intelligent Robots and Systems*, 2009, pp. 2922–2927.